minerals

MDPI

Article

Microstructural Deformation and the Age of Monazite-(Ce) from Diatectite Granite in the Jarva-Varaka Structure (Kola Region, Russia)

Tatiana Kaulina [1,*], Vladimir Shilovskih [2], Lyudmila Nerovich [1], Yevgeny Savchenko [1], Vladimir Bocharov [2], Lyudmila Lialina [1] and Vadim Il'chenko [1]

[1] Geological Institute of Kola Science Centre of RAS, Apatity 184209, Russia; nerovich@geoksc.apatity.ru (L.N.); ye.savchenko@ksc.ru (Y.S.); l.lyalina@ksc.ru (L.L.); v.ilchenko@ksc.ru (V.I.)
[2] "Geomodel" Resource Center, Saint-Petersburg State University, Saint-Petersburg 199037, Russia; vvshilovskih@gmail.com (V.S.); bocharov@molsp.phys.spbu.ru (V.B.)
* Correspondence: kaulina@geoksc.apatity.ru; Tel.: +7-9210427983

Abstract: Microstructural deformation and the age of monazite (Ce) from diatectite granite of the presumably impact Jarva-Varaka structure in the Kola Region (northeastern Fennoscandian Shield) are presented. Biotite diatectite granite forms lenses in the aluminous gneisses of the Kola group hosting the 2.5-Ga-layered Jarva-Varaka Massif (JVM). A sample of biotite granite was collected northeast of the Jarva-Varaka Massif near the earlier described pseudotachylitic breccias. BSE images revealed primary domains in monazite grains with rhythmic euhedral zoning and secondary altered domains. Backscattered electron diffraction maps of monazite grains document the development of deformation twins along {100} and {001} and plastically deformed domains with a maximum misorientation of up to 10°. Newly formed areas of recrystallization (neoblasts) cut the twins and plastically deformed domains. Monazite yielded a U-Pb age of 2706 ± 10 Ma (ID-TIMS method), which defines the crystallization age of the host diatectite granite coeval to the 2.76–2.70 Ga metamorphism of the Kola gneisses. A similar age of 2734 ± 139 Ma (ThO2*–PbO isochron) was obtained for primary monazite domains by the chemical U-Th-total Pb isochron method (CHIME). Domains altered under late hydrothermal processes yield CHIME ages of 1796–1723 Ma. Monazite neoblastic domains are close to primary domains in chemical composition and yielded CHIME ages of 2550–2519 Ma, reflecting probably an influence of the JVM formation. The data obtained are insufficient to confirm the impact origin of the Jarva-Varaka structure, which requires further investigation.

Keywords: deformation microstructure; monazite; shock metamorphism; CHIME dating; diatectite granite; EBSD; Kola region

Citation: Kaulina, T.; Shilovskih, V.; Nerovich, L.; Savchenko, Y.; Bocharov, V.; Lialina, L.; Il'chenko, V. Microstructural Deformation and the Age of Monazite-(Ce) from Diatectite Granite in the Jarva-Varaka Structure (Kola Region, Russia). *Minerals* **2023**, *13*, 1325. https://doi.org/10.3390/min13101325

Academic Editor: Bernhard Schulz

Received: 4 September 2023
Revised: 6 October 2023
Accepted: 9 October 2023
Published: 13 October 2023

1. Introduction

Meteorite bombardment could have made a significant contribution to the formation of the early Earth's crust (for example, [1–3]). However, both the identification and investigation of the most ancient (Precambrian) terrestrial impact structures are hampered by their inevitable degradation due to subsequent metamorphic, tectonic, and weathering processes. Only a few Precambrian impact structures older than 1.6 Ga are currently known, including Vredefort (2023 ± 4 Ma—[4]) in South Africa, Sudbury (1850 ± 3 Ma—[5]) in Canada, Yarrabubba (2229 ± 5 Ma—[6,7]) in Australia, Dhala (proposed age of 2.44–2.24 Ga—[8]) in India, and possibly Suavjärvi (~2.4 Ga—[9]) in Russia. The poor preservation of meteorite impact traces has been addressed by developing a set of diagnostic criteria for identifying impact structures on the Earth's surface and distinguishing them from similar structures created by endogenous geological processes [10–12]. Diagnostic evidence for impact events is more likely to be found in the target rocks that were affected by the impact, since the meteorite itself is mainly destroyed in an impact event [3]. Shock deformation effects

include shatter cones, specific planar microdeformation features in minerals, isotropization (e.g., formation of diaplectic glasses), and phase changes (high pressure phases and melting) [10,12]. Much better impact traces are preserved in accessory minerals, such as zircon, monazite, etc., which can be used in the study of old, deeply eroded, and metamorphically overprinted impact structures [13–19].

In the 1980s, in the Kola-Karelian region of the Fennoscandian Shield, several structures with brecciated rocks were considered potentially diamondiferous impact structures; however, since diamonds have not been found, the investigations were terminated, and none of these structures were confirmed as astroblemes. Now, only one confirmed impact crater is known in the region—Janisjärvi of 725 ± 5 Ma [20]. The origin of the 2.4 Ga Suavjärvi structure [9] is under question since investigations in 2012 provided no evidence in support of an impact origin [21].

The layered Jarva-Varaka Massif (JVM), located in the Monchegorsk ore area of the Kola region (Figure 1), has gained the attention of researchers as it is different from other mafic layered intrusions from this area. Recent studies have shown [22,23] that according to the significant amount of granophyre in all lithologies, petrographic and geochemical composition, a comparable thickness of the igneous complex (~2000 m), and brecciated rocks at the base, the JVM is very similar to the well-studied 1.85 Ga Sudbury Igneous Complex (SIC), for which an impact origin was assumed [24,25]. The results obtained gave rise to a hypothesis on an impact origin for the JVM [22,23]. The presence of granophyre in all lithologies of the JVM suggests massif crystallization from a melt enriched in crustal material. The norite contains micro-xenoliths of the host alumina gneisses, transformed into rocks of the high-grade hornfels facies. The formation of hornfelses, at the relatively small size of the massif, could have occurred if the xenoliths were entrained by a melt under near-surface conditions and the melt was hot enough to cause the formation of hornfelses. Spinifex-like structures in diorites of the marginal zone at the contact of the JVM indicate very rapid cooling of a high-temperature melt, which is also typical of near-surface conditions [23]. About 1/3 of zircons from granophyre norite (sample 1/114 from [23]) with numerous inclusions of sillimanite and plagioclase were most likely entrained from the host aluminous gneisses. Raman spectroscopy and X-ray studies revealed the fully amorphous structure of zircon rims with sillimanite and plagioclase inclusions. The data is hard to explain by metamictization of old zircons since the U content ($\leq$600 ppm) is not enough for pronounced metamictization, while sillimanite and plagioclase do not contain radioactive elements at all. It better fits the mineral transformation into diaplectic glasses due to shock metamorphism that affected the gneisses [26].

These data stimulated further investigations aimed at searching for shock features within host gneisses and granitoids, which would have been the target rocks. In 2018, during field investigations, pseudotachylitic breccia and thin lenses of glassy material were found within gneisses northeast of the Jarva-Varaka Massif (Figure 1). Quartz with planar fractures and kink-banding structures in biotite and clinozoisite were also observed in granitoids and gneisses hosting the breccia [23]. The kink-band structures are quite frequent in micas within tectonic deformation zones but are rare in clinozoisite, where they may represent evidence of impact-related damage. Even if pseudotachylites are not undeniable signs of an impact event, multiple planar fractures (PF) in quartz are definitely the product of impact-generated shock waves ([12] and references therein).

Here we present microstructural deformation and CHIME (chemical U-Th-total Pb isochron method) age of monazite-(Ce) ((Ce,La,Nd…)[PO_4]) from a sample of diatectite granite northeast of the Jarva-Varaka Massif within the host aluminous gneisses of the Kola group (Figure 1).

Monazite has been reported as a shocked mineral at several impact structures, including Haughton in Canada [27], Araguainha in Brazil [28,29], Yarrabubba and Woodleigh in Australia [29,30], and Vredefort in South Africa [17,29–33], and it was interesting to compare the obtained results.

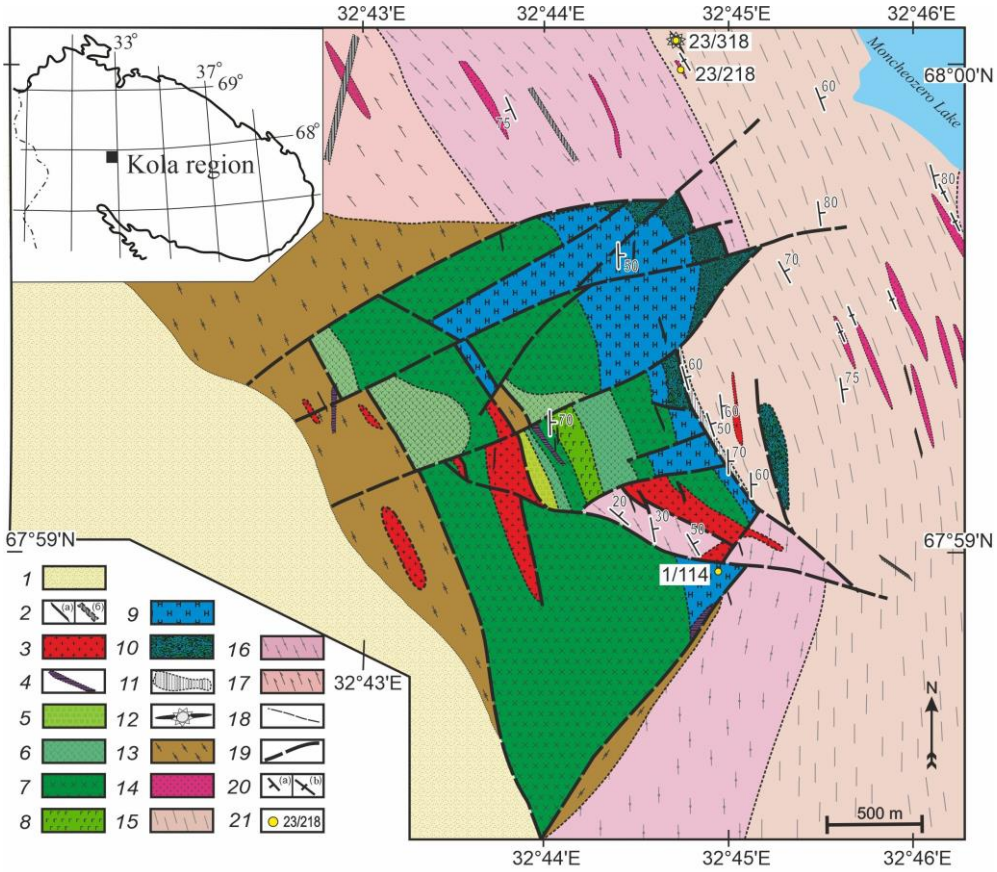

Figure 1. Schematic geological map of the Jarva-Varaka structure with sample locations. 1—Quaternary deposits; 2–11—Paleoproterozoic 2—dolerite dykes; 3—microcline granites; 4–10—rocks of the Jarva-Varaka Massif: 4—porphyritic dykes, 5–10—granophyre rocks: 5—granodiorite, 6—quartz diorite, 7—hypersthene diorite, 8—pigeonite and augite diorite, 9—norite, 10—marginal diorite; 11—brecciated granitic gneisses; 12—pseudotachylitic breccia; 13–17—Archaean. 13—biotite-amphibole dioritic gneisses; 14—sheet-like granitoid bodies; 15–17—Kola Group: 15—sillimanite-biotite and sillimanite-garnet-biotite gneisses with kyanite and staurolite; 16—alternation of biotite, garnet-biotite ± sillimanite, amphibole-biotite, epidote-biotite gneisses, amphibolites and amphibole-magnetite quartzites; 17—biotite gneisses with subordinate amphibole-biotite gneisses and rare amphibolite bodies; 18—boundaries; 19—faults; 20—schistosity and banding inclined (a) and vertical (b); 21—sample location and number; Samples discussed in the text: 1/114—granophyre norite [23,26]; 23/318—pseudotachylitic breccia [23], 23/218—biotite diatectite granite (this study).

2. Geological Setting

The Jarva-Varaka layered massif is located in the Monchegorsk ore district of the Kola region of the NE Fennoscandian Shield (Figure 1). The massif is 1.7 × 2.2 km in size [34] with a thickness of about 2 km. The JVM consists of a differentiated series: norite, hypersthene diorite, pigeonite-augite diorite, quartz diorite, and granodiorite. Lithologies of the Massif contain granophyre (Qtz + Pl + Kfs) in different proportions [23]. The dyke complex is represented by pyroxene-plagioclase porphyrites. Fracture tectonics is widely manifested within the JVM.

The host rocks for the Jarva-Varaka Massif are Archean aluminous gneisses of the Kola group with numerous sheet-like bodies of biotite granite, alaskite pegmatite, and pegmatoid leucoplagiogranite. Small and large veins of microcline granite cut the Massif and contain xenoliths of the massif rocks. Except for leucoplagiogranite, which is an A-type anorogenic

granitoid, other granites are of the crustal-anatectic S-type [35]. When we use the term "Jarva-Varak structure", we mean the Massif itself and host gneisses and granitoids.

An age of the Massif is accepted as 2.5 Ga based on the age of quartz diorite obtained by the U-Pb ID-TIMS method on zircon (2496 ± 9 Ma—[34]) and the 2498 ± 6 Ma age of pigeonite-augitic diorite obtained by the U-Pb SHRIMP-II method on baddeleyite and zircon [26].

Pseudotachylitic breccia was discovered northeastward of the massif in gneisses of the Kola group (Figure 1) (sample 23/318 in [23] with coordinates N68°00′01.87″ E32°44′47.07″—WGS 84). The pseudotachylitic breccia extends as a narrow band among aluminous gneisses and granites for about 50 m in the NW 330–335° direction. The width of the band decreases towards NW from 1 m to 20 cm. Clasts of granites and gneisses, quartz and plagioclase fragments are embedded into glassy cement with a cryptocrystalline structure. For more details see [23].

Monazite grains were separated from biotite diatectite granite (sample 23/218—N68°00′01.45″ E32°44′46.95″), which forms a lens in the Kola gneisses and is located northeast of the Jarva-Varaka Massif near the earlier described pseudotachylitic breccia (Figure 1). Granites of this type form a group of sheet-like bodies up to 1 m thick, sub-concordant with the schistosity of the host aluminous gneisses. Granites are locally and weakly foliated, but mainly have a massive structure.

3. Materials and Methods

3.1. Materials

Sample 23/218 (N68°00′01.45″ E32°44′46.95″) is represented by massive biotite granite with inequigranular texture and rare large porphyritic microcline grains (Figure 2). The sample is composed of quartz (40%), plagioclase (30%), microcline (20%), biotite (5%), and muscovite (3%). Major minerals (quartz, plagioclase, and microcline) are represented by two generations. The first generation consists of rare irregularly shaped quartz grains of up to 3 mm in size and large microcline grains up to 6 mm with inclusions of plagioclase.

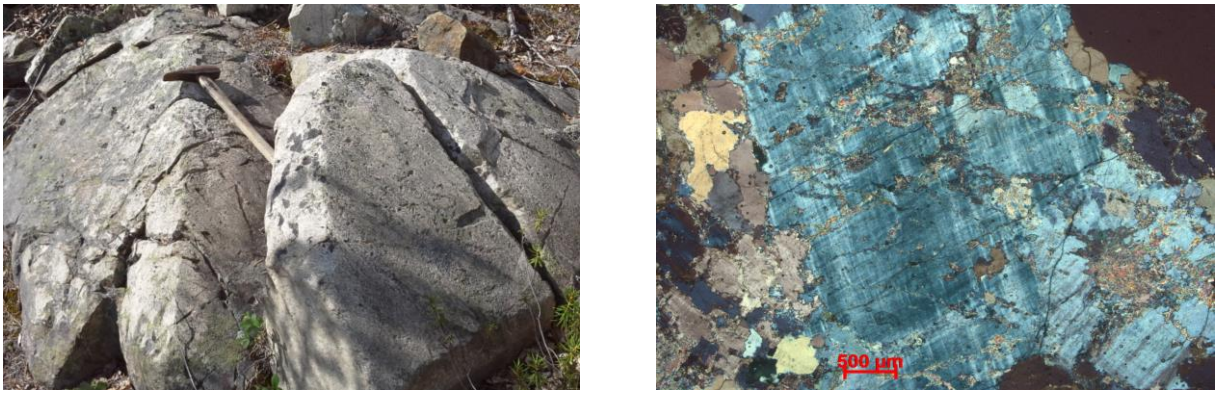

(**a**) (**b**)

Figure 2. (**a**) field photograph of bodies of biotite granite of sample 23/218. (**b**) thin section of the sample with inequigranular texture and large microcline grain in the center, crossed polarized light.

The second generation of these minerals is represented by smaller grains of irregular shape: quartz of 0.1–1.7 mm in size, plagioclase of up to 1.5 mm observed in the groundmass, and microcline of 0.5–3 mm. Muscovite and biotite are developed in intergranular space together with sericite.

Monazite, separated from the sample of biotite granite, is represented by sub-isometric yellowish grains, 150–200 µm in size.

3.2. Methods

Monazite grains from the sample were embedded in epoxy, ground down to about half of their thickness, and polished. The backscattered electron (BSE) images, composition of inclusions, and chemical composition of neoblastic domains in monazite were studied by

a LEO-1450 Scanning Electron Microscope (Carl Zeiss Microscopy, Oberkochen, Germany) equipped with an Aztec UltimMax 100 (Oxford Instruments, Oxford, UK) energy dispersive spectrometer (EDS) at the Geological Institute, Kola Science Center of Russian Academy of Sciences (GI KSC RAS) in Apatity, Russia. EDS analyses were carried out with an accelerating voltage of 20 kV, a probe current of 2 nA, and a spectrum accumulation time of 100 s. Analytical errors (2σ) were 0.01–0.1%, and the average detection limit was 0.03%.

The chemical composition of monazite by means of the X-ray microanalyzer Cameca MS-46 (Cameca, Gennevilliers, France) was studied at the GI KSC RAS (Apatity) in wavelength dispersive spectroscopy (WDS) mode. The accelerating voltage for most elements was 22 kV; for Pb, Th, and U, it was 32 kV; the beam diameter was 1–2 μm; the probe current was 20–40 nA; the accumulation time was 10 s for peaks and the background on both sides of the peak (4–5 measurements were taken at each point). Analytical lines (and standards): SiKα and CaKα (wollastonite), PKα (fluorapatite), YLα ($Y_3Al_5O_{12}$), LaLα1 (LaSe), CeLα1 (CeS), PrLβ1 ($Pr_3Al_5O_{12}$), NdLα1 ($LiNd(MoO_4)_2$), SmLα1 ($SmFeO_3$), GdLα1 (GdS), DyLα1 ($Dy_3Al_5O_{12}$), PbLα1 ($PbMoO_4$), ThLα1 (thorite), ULα1 (UO_2). The detection limits of elements (2σ) are for Si and P—0.05%, Ca—0.03%, La, Ce—0.05%, Y, Pr-Du, Pb, Th, and U—0.1%. The measurement uncertainties did not exceed 1%, 2.5%, and 5% for concentrations of 10 wt.%, 1 wt.%, and 0.25 wt.%, respectively.

Electron backscatter diffraction (EBSD) was used to reveal deformed and undeformed domains in the monazite crystals. EBSD mapping was carried out in the "Geomodel" Centre of St-Petersburg University Scientific Park (Saint-Petersburg, Russia). The epoxy mount with monazite grains was additionally polished by Ar ion etching for 10 min (Oxford IonFab 300) for the flattest possible surface required for EBSD analysis. EBSD mapping was carried out using a Hitachi S-3400N scanning electron microscope equipped with an Oxford HKLNordlys EBSD detector. Operating conditions were as follows: accelerating voltage was 30 kV and beam current was 2 nA. Diffraction maps were prepared with an exposure of 90 milliseconds per point with a step of 200–330 nm. The Oxford Instruments AZtecHKL analysis software (v2.1) was used to identify the crystal orientation from the Kikuchi pattern according to the monazite crystal structures from the ICSD (9001647) database after conversion of P1 21/n 1 for presentation into P1 21/c 1.

Monazite grains were dated by the classic U-Pb (ID-TIMS) method in the laboratory for geochronology and isotope geochemistry of GI KSC RAS (Apatity). Digestion of minerals, U, and Pb extraction followed the method of Krogh [36]. The measurements were performed on a Finnigan MAT 262 mass spectrometer (for details see [37]).

The age of local monazite domains was defined by the chemical U-Th-total Pb isochron method (CHIME) [38] according to the measured content of Th, U, and Pb oxides in monazite. Because monazite is rich in Th and U, radiogenic Pb (*Pb) accumulates very quickly and reaches, in about 100 Ma, a level where precise measurements can be performed with an electron microprobe [39,40]. Age calculations were carried out using the original program [40] based on the Isoplot/Ex software 3.70–4.15 [41].

4. Results

4.1. Chemical Composition of Monazite (WDS Data)

Monazite grains are characterized by internal heterogeneity associated with the difference in composition and observed on BSE images in the form of light gray and dark gray domains (Figure 3). The monazites analyzed are Ce-rich (Ce_2O_3 up to 31.6 wt%) and have high La_2O_3 (14.2–18.2 wt%), Nd_2O_3 (7.62–9.44 wt%), and ThO_2 (4.87–12.3 wt%) contents. The chemical composition of monazite-(Ce) is shown in Table 1.

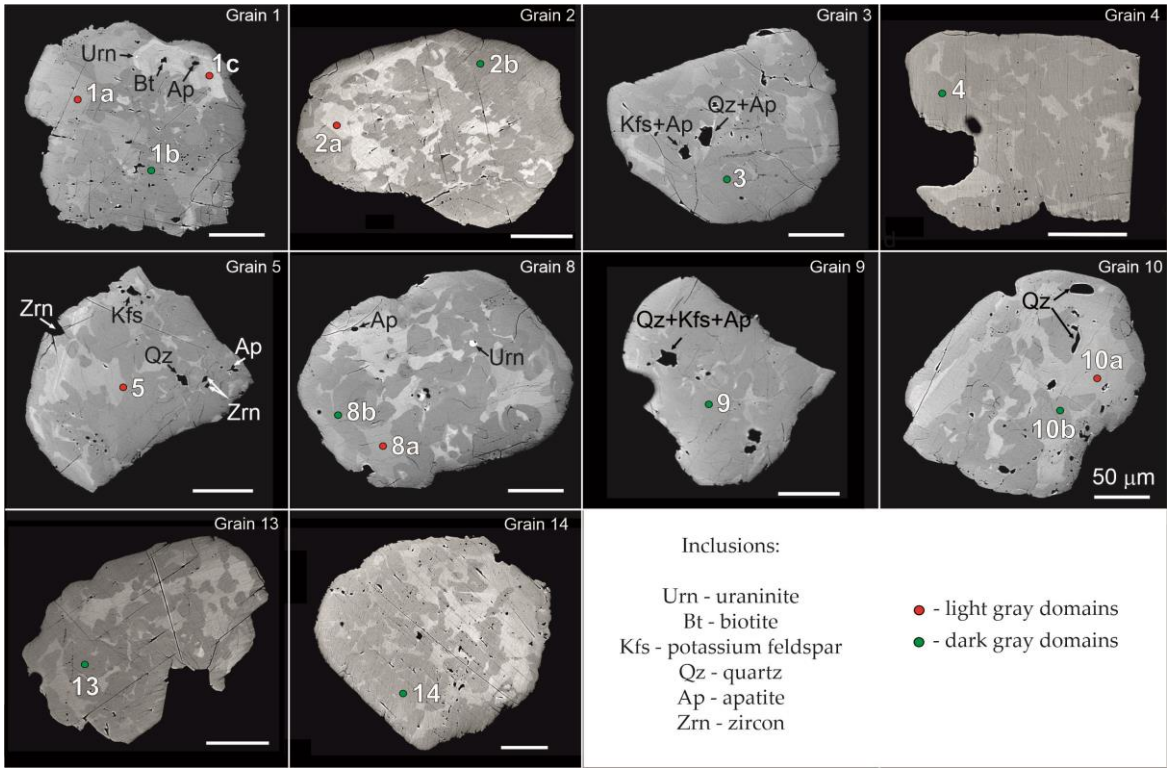

Figure 3. BSE images showing heterogeneous internal structure of monazite-Ce grains with points of microprobe analysis. Arrows show inclusions of uraninite, biotite, potassium feldspar, quartz, apatite and zircon. Scale bar—50 μm. Red spots correspond to light gray domains; green spots correspond to dark gray domains.

Table 1. Chemical composition (WDS data, wt%) of monazite-(Ce) from diatectite granite (sample 23/218) and chemical formulas for light gray and dark gray domains.

Components	Number of Analysis														
	1a	**1b**	**1c**	**2a**	**2b**	**3**	**4**	**5**	**8a**	**8b**	**9**	**10a**	**10b**	**13**	**14**
SiO_2	0.65	0.12	1.64	1.90	0.18	0.10	0.24	0.11	0.66	0.05	0.11	0.89	0.26	0.27	0.23
P_2O_5	26.5	29.3	27.0	26.4	28.7	29.0	29.2	30.2	27.5	27.6	29.0	29.0	30.0	29.4	29.0
CaO	0.85	1.71	1.08	1.19	1.93	1.89	1.94	2.01	0.91	1.78	1.93	1.09	2.00	1.83	1.81
Y_2O_3	0.78	2.04	1.51	1.53	3.36	2.28	3.18	1.39	2.42	0.74	2.01	1.04	2.14	2.98	2.98
La_2O_3	17.3	15.9	15.8	14.4	14.2	16.3	14.6	15.5	18.2	15.1	15.2	16.2	14.7	14.8	14.8
Ce_2O_3	31.6	29.0	29.6	27.9	27.6	28.4	28.0	28.2	28.8	31.2	28.2	30.0	27.6	28.1	28.1
Pr_2O_3	3.11	2.49	2.56	2.39	2.43	2.24	2.27	2.43	2.82	2.51	2.57	2.30	2.27	2.31	2.35
Nd_2O_3	9.44	8.59	7.62	7.75	7.62	8.53	7.66	8.46	9.03	8.53	8.57	8.57	8.59	7.77	7.72
Sm_2O_3	1.45	1.62	1.34	1.40	1.64	1.17	1.34	1.16	1.47	1.36	1.40	1.18	1.29	1.55	1.59
Gd_2O_3	1.18	1.22	0.70	0.86	1.23	1.19	0.94	1.09	1.10	1.15	1.29	0.92	1.14	1.09	1.22
Dy_2O_3	0.27	0.48	0.00	0.00	0.53	0.49	0.00	0.27	0.17	0.57	0.50	0.26	0.48	0.00	0.53
PbO	0.83	1.21	1.48	1.52	1.59	1.29	1.72	1.32	0.82	1.25	1.45	0.94	1.38	1.56	1.44
ThO_2	6.04	5.06	10.9	12.3	6.50	4.87	6.54	5.75	5.45	5.54	5.22	6.39	6.73	6.81	6.47
UO_2	0.00	0.86	0.41	0.55	1.95	1.26	2.10	0.83	0.00	0.96	1.68	0.00	1.03	1.68	1.45
Total	100.0	99.6	101.7	100.0	99.5	99.0	99.8	98.8	99.3	98.4	99.1	98.7	99.7	100.1	99.6

Light gray domains (spots 1a, 1c, 2a, 5, 8a, 10a), $(Ce_{0.41–0.48}REE_{0.43–0.53}Ca_{0.04–0.09}Th_{0.05–0.11}Pb_{0.01–0.02}U_{0–0.01})_{1.0–1.09}[(P_{0.91–1.00}Si_{0–0.08})_{0.95–1.01}O_4]$; Dark gray domains (spots 1b, 2b, 3, 4, 8b, 9, 10b, 13, 14), $(Ce_{0.40–0.47}REE_{0.44–0.49}Ca_{0.07–0.08}Th_{0.04–0.06}Pb_{0.01–0.02}U_{0.01–0.02})_{1.01–1.07}[(P_{0.96–0.99}Si_{0–0.01})_{0.96–1.0}O_4]$.

Light gray domains (analyses 1a, 1c, 2a, 5, 8a, 10a in Figure 3) can be considered primary since they preserve rhythmic euhedral zoning (grains 1, 2, 5 in Figure 3), which, together with apatite and biotite, can be considered as primary growth zoning. Dark

gray domains (analyses 1b, 2b, 3, 4, 8b, 9, 10b, 13, 14) have irregularly curved boundaries, characteristic for fluid influence, and are considered secondary.

Light gray domains differ from the dark ones due to their very low UO_2 (below detection limit), low PbO, Dy_2O_3, and CaO, and higher SiO_2, La_2O_3, and ThO_2 (Table 1). Inclusions of quartz, apatite, biotite, and potassium feldspar suggest the formation of monazite-(Ce) at the late stage of granite crystallization.

4.2. EBSD Mapping

The EBSD mapping reveals a deformational microstructure in some monazite grains. These grains are composed of domains with a slightly different crystallographic orientation and are cut by sets of lamellar twins (Figure 4).

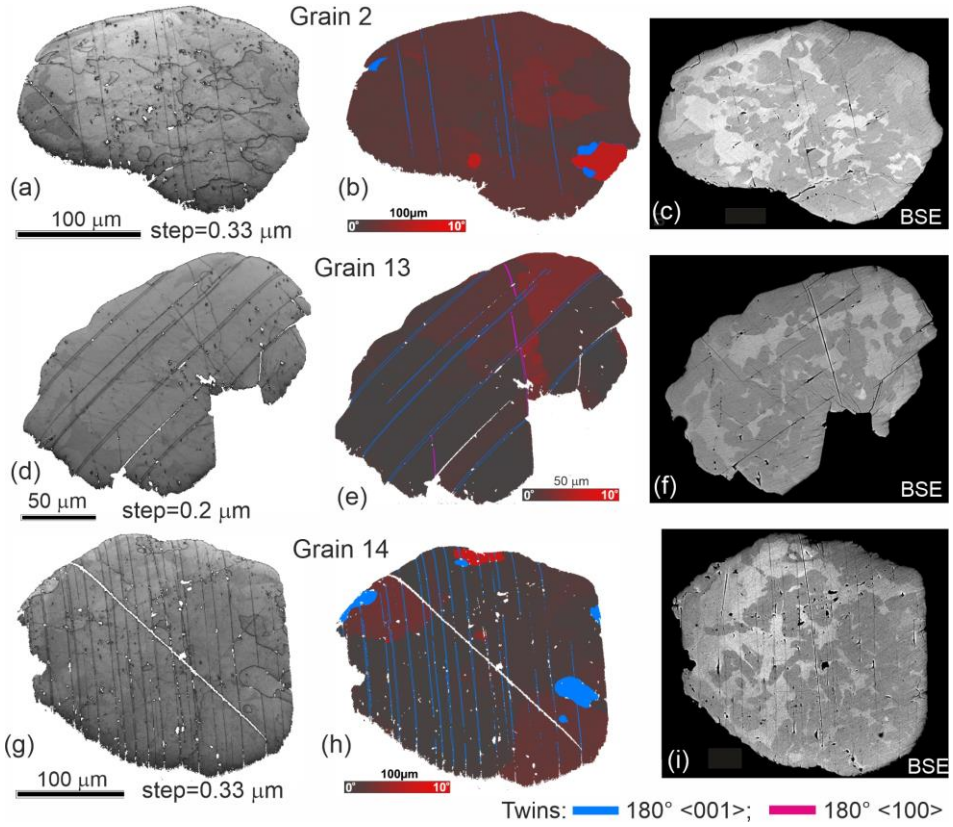

Figure 4. Deformed monazite from sample 23/218 from diatectite granite of the Jarva-Varaka structure. Contrast maps (diffraction quality) (**a**,**d**,**g**). Maps of intragrain misorientations (**b**,**e**,**h**) show the distortion of domains relative to the average grain orientation with a maximum local misorientation of 10°. Blue (and magenta in grain 13) lines are boundaries of twins. Blue domains are neoblasts. BSE images (**c**,**f**,**i**).

The boundaries of twins and subgrains are clearly visible on diffraction pattern quality maps (Figure 4a,d,g). Maps of intragranular misorientations show a slight rotation of domains relative to the average grain orientation (Figure 4b,e,h). Up to 11 subdomains with different orientations were marked with a maximum misorientation of up to 10°.

Three grains contain sets of twins, which are developed along {001} and {100} with 180° disorientation relationships (Figure 4b,e,h). The dominant twin set forms along {001} in all three grains (blue boundaries at Figure 4); grain 2 also contains twins along {100} (magenta boundaries in Figure 4e).

Newly formed domains (neoblasts) were also found (blue subdomains in Figure 4b,h), which are not deformed and cut the twin sets and plastically deformed domains. These neoblastic domains range in diameter from 5 to 35 μm and have typically rounded, lobate

forms. They are highly misoriented relative to the host grain and have specific crystallographic orientation consistent with the orientation of twins.

Irregular domains with different intensity in the BSE (Figure 4c,f,i) are superimposed on twins and plastically deformed areas, indicating later processes.

4.3. U-Pb ID-TIMS and CHIME Dating of Monazite

Four monazite fractions of 150–200 µm (points M_1 and M_2 in Figure 5a) and 100–150 µm (M_3 and M_4) were hand-picked for U-Pb ID-TIMS analysis. We tried to choose very pure grains, although monazite grains in general were muddy and fissured. That is why the data points for the finer monazite fraction are rather discordant. Four fractions yielded an upper intercept age of 2706 ± 10 Ma (Figure 5a, Table 2). Low MSWD = 0.08 shows small geochemical variations between monazite grains.

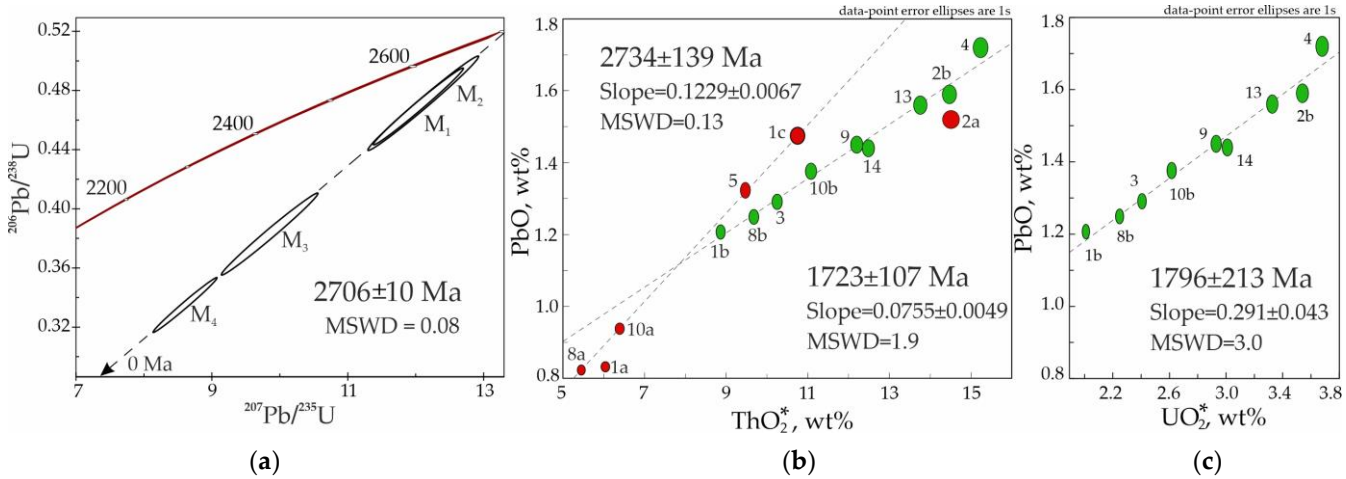

Figure 5. Th-U-Pb age of monazite from diatectite granite (sample 23/218). (**a**)—U-Pb concordia diagram, (**b**,**c**)—CHIME isochrons: (**b**)—ThO_2*-PbO and (**c**)—UO_2*-PbO for local monazite domains. The analyses numbers in (**b**,**c**) follows numeration in Figure 3 and Table 1.

Table 2. U-Pb isotope data for monazite from diatectite granite (sample 23/218).

No	Sample Weight, mg	Concentration, ppm		Pb Isotope Composition			Isotope Ratio				Rho	Age, Ma
		Pb_{rad}	U	$\frac{^{206}Pb}{^{204}Pb}$	$\frac{^{206}Pb}{^{207}Pb}$	$\frac{^{206}Pb}{^{208}Pb}$	$\frac{^{207}Pb}{^{235}Pb}$	2σ, %	$\frac{^{206}Pb}{^{238}Pb}$	2σ, %		$\frac{^{207}Pb}{^{206}Pb}$
M_1	2.8	9432	8289	14,000	5.359	0.6197	12.030	4.5	0.4697	4.5	0.99	2705 ± 1
M_2	2.4	10,184	8807	17,000	5.356	0.6071	12.099	5.5	0.4718	5.5	0.99	2707 ± 1
M_3	4.3	8459	9272	13,900	5.348	0.6396	9.841	5.9	0.3835	5.9	0.99	2708 ± 1
M_4	3.5	7198	9023	12,600	5.354	0.6407	8.598	4.5	0.3356	4.5	0.99	2705 ± 1

Age calculations for individual monazite domains from the EMPA content of U, Th, and Pb (analyses in Table 1) gave two results. An age of 2734 ± 139 Ma was obtained for light gray (primary) domains according to ThO_2*–PbO isochron (Figure 5b), which is consistent with the ID-TIMS monazite age of 2710 ± 10 Ma. UO_2*–PbO isochron for the same domains was not calculated because of low U concentrations, which are below the detection limits in three grains (Table 1).

The dark gray (secondary) domains yielded an age of 1723 ± 107 Ma according to ThO_2*–PbO isochron and 1796 ± 213 Ma according to UO_2*–PbO isochron (Figure 5b,c).

4.4. Chemical Composition (EDS Data) and CHIME Age of Monazite Neoblastic Domains

The chemical composition of neoblastic domains revealed by EBSD (Figure 6) was studied by the EDS method due to their small size (5–35 µm) and is shown in Table 3.

Neoblastic domains also show internal heterogeneity visible in BSE (Figure 6), but in total, all of the neoblasts have a chemical composition similar to that of the primary domains (Figure 7). The difference lies in the wider variations in SiO_2, ThO_2, and UO_2 concentrations.

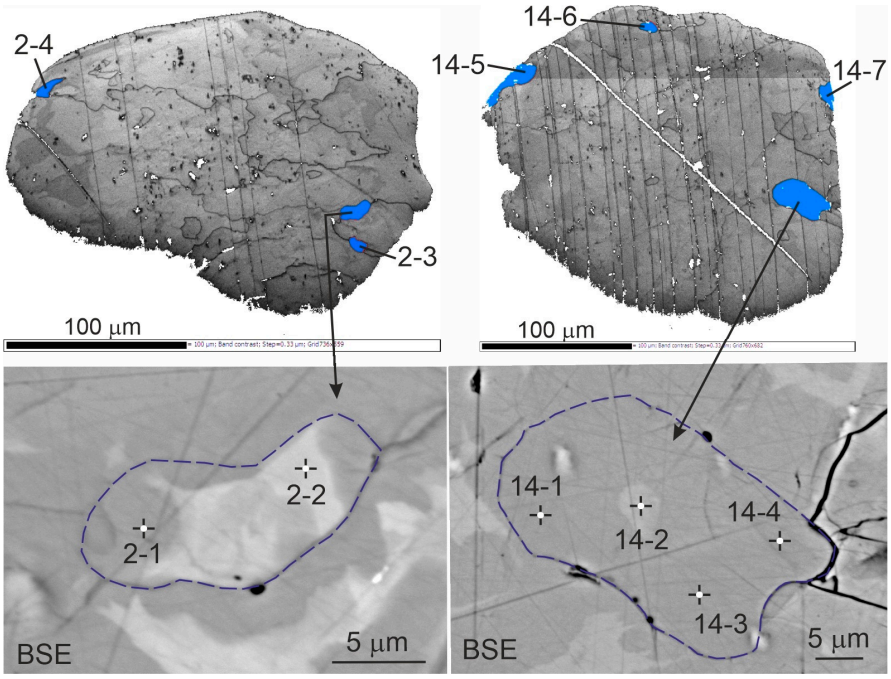

Figure 6. Neoblastic domains in monazite grains from diatectite granite (sample 23/218) with points of microprobe analysis.

Table 3. Chemical composition (EDS data, wt%) of neoblastic domains in monazite grains from the sample 23/218 of diatectite granite.

Components	Number of Analysis										
	2-1	**2-2**	**2-3**	**2-4**	**14-1**	**14-2**	**14-3**	**14-4**	**14-5**	**14-6**	**14-7**
SiO_2	0.00	2.25	0.26	0.21	0.18	0.76	0.00	0.19	0.20	0.00	0.18
P_2O_5	29.7	25.4	29.4	29.4	29.3	28.2	29.0	28.4	28.4	28.5	26.9
CaO	2.24	1.40	2.23	2.08	1.75	0.96	1.83	1.85	2.03	1.82	1.70
Y_2O_3	2.88	1.56	3.41	3.47	3.24	1.77	3.29	3.14	2.29	3.08	2.82
La_2O_3	13.9	14.2	13.8	14.2	14.6	16.5	14.7	14.6	13.8	14.2	14.6
Ce_2O_3	27.6	26.7	26.7	27. 5	28.1	31.2	28.2	28.1	28.0	27.7	27.6
Pr_2O_3	2.37	2.33	2.37	2.37	2.45	2.54	2.39	2.6	2.51	2.41	2.35
Nd_2O_3	7.87	7.04	7.61	7.74	7.82	7.98	7.76	7.77	8.11	7.95	7.46
Sm_2O_3	1.57	1.25	1.52	1.43	1.65	1.42	1.59	1.51	1.44	1.62	1.34
Gd_2O_3	1.05	0.86	1.19	0.79	1.04	0.79	0.98	1.06	1.03	1.18	1.04
Dy_2O_3	0.00	0.00	0.73	0.00	0.55	0.00	0.00	0.59	0.00	0.6	0.50
PbO	2.00	1.76	1.76	1.78	1.43	0.86	1.46	1.44	1.56	1.43	1.25
ThO_2	7.45	14.6	8.28	7.12	6.30	6.46	6.37	6.31	6.86	6.45	6.29
UO_2	2.40	0.59	1.82	2.06	1.67	0.59	1.68	1.58	1.99	1.67	1.32
Total	101.6	100.0	101.1	100.1	100.0	100.0	99.2	99.2	98.2	98.6	95.3
$(Ce_{0.38–0.46}REE_{0.41–0.48}Ca_{0.04–0.09}Th_{0.06–0.14}Pb_{0.01–0.02}U_{0.01–0.02})_{1.02–1.06}[(P_{0.89–0.98}\ Si_{0–0.03})_{0.97–0.98}O_4]$											
Age, Ma [1]	2662	2365	2567	2640	2511	2256	2555	2601	2434	2503	2476

[1] Th-U-Pb age was calculated by algorithm of Montel [39]. The analyses numbers follow numeration in Figure 6.

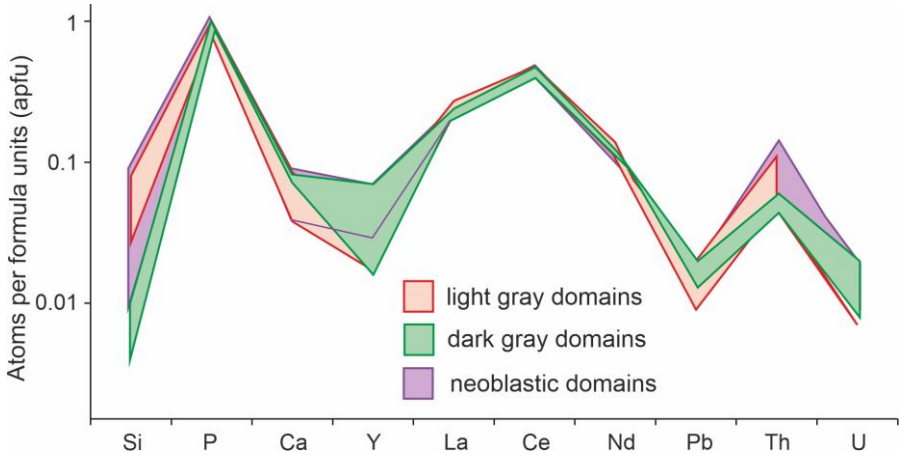

Figure 7. Composition of different domains in the monazite grains (diatectite granite sample 23/218).

The contents of U, Th, and Pb oxides in monazite neoblasts were measured in order to estimate the age of the process that produced them (Table 3).

The age of neoblastic domains was calculated using the Montel algorithm [39] and CHIME method with the construction of isochrones (Figure 8). The obtained Montel ages for each point varied from 2256 Ma to 2662 Ma (Table 3).

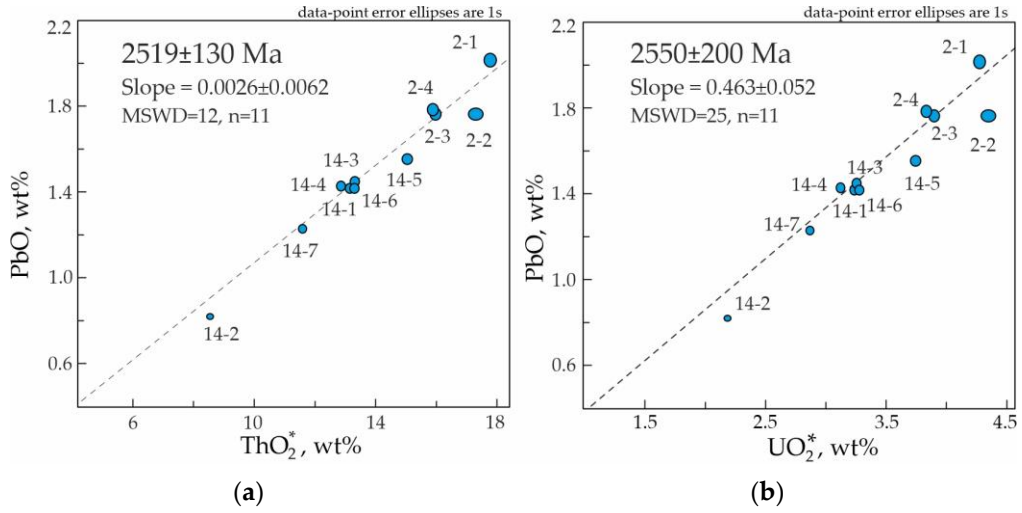

Figure 8. CHIME ThO2*-PbO (**a**) and UO2*-PbO (**b**) isochrons for neoblastic domains in monazite grains from diatectite granite (sample 23/218).

In the ThO_2*-PbO and UO_2*-PbO diagrams, the data points display a sufficiently large scatter (Figure 8), which is consistent with age variations in Table 3. CHIME isochrones calculated via virtual zero point determined the ages of 2519 ± 130 (ThO_2*-PbO) and 2550 ± 200 Ma (UO_2*-PbO) (Figure 8). According to the Suzuki method [38], all isochrons pass through zero; therefore, with a scatter of points, as in our case, we may use the zero point when calculating.

5. Discussion

5.1. EBSD Pattern

Deformation microstructure, including twins, plastically deformed domains, and recrystallized domains (neoblasts), is a common feature of monazites that have been deformed either in tectonic or shock metamorphic environments (for example, [17] and references therein). Impact-related microstructural deformation has been described in shock-deformed monazite from the well-known impact structures such as Vredefort in

South Africa, Yarrabubba and Woodleigh in Australia, and Araguainha in Brazil [27–33]. Similar deformational twins and dynamically recrystallized neoblasts in monazite have been documented in tectonic environments [42]. Observations from tectonically deformed monazite revealed twins along (100), (001), {120} and {122} [42]. Shocked monazite grains were shown to contain additional deformation twins parallel to (101), {110}, (102), {212}, {120} and two irrational planes containing [011] and [110] shear directions [17,30].

Twinning, as the most common deformation microstructure reported within monazite, can be obtained even under room-temperature conditions in indentation experiments [43], but the formation of neoblastic domains by dynamic recrystallization requires a temperature increase [42]. The sample of tectonically deformed monazite described in [42] came from the Sandmata Complex in India with granulite-facies metamorphism (~7–10 kbar and ~800–900 °C), reworked by high-strain mylonitic shear zones, where deformation occurs at high temperatures. Our sample of diatectite granite is represented by a massive rock with no signs of tectonic deformation. The Jarva-Varaka structure, together with the whole Monchegorsk ore area, does not belong to a highly strained terrain and has not undergone high-pressure or high-temperature regional metamorphism after 2.7 Ga. The host alumina gneisses have been highly metamorphosed during the Archean period. The last stage of regional metamorphism in the area occurred 2.76–2.7 Ga ago, which produced the coeval diatectite granites with no signs of later superimposed tectonic deformation or metamorphism. The next tectonic event in the area happened locally 2.0–1.9 Ga ago and resulted in the formation of the Monchetundra fault, which is located 12 km southwest of the Jarva-Varaka structure. The only event that could have affected the granites is the formation of the Jarva-Varaka Massif, which was too small to sufficiently heat the host rocks.

Thus, it is difficult to connect microstructural deformation in monazite-(Ce) from diatectite granite with tectonic processes in the area. However, in any case, the absence of shock-specific twins in the monazite grains provides no conclusive evidence to support an impact origin for the Jarva-Varaka structure at this stage of the research.

We can also add that, for example, monazites from granite and micaschist lithoclasts of impact breccia in the Nördlinger Ries impact crater display a combination of strictly parallel straight cracks interpreted as lamellae structures of shock deformation, but no neoblasts or specific twins have yet been detected [44]. The authors associate this with the intermediate shock levels at the sampled outcrop.

5.2. Monazite Age

Monazite grains, in general, retain the age of the rock and do not reflect the age of subsequent events such as impact [29–31,44] or tectonic deformation [42]. U-Pb ID-TIMS dating determined the monazite crystallization age as 2.7 Ga. The U-Pb ages of each fraction are not concordant, indicating lead loss that is lower for coarse fractions (M_1 and M_2). Quartz, apatite, biotite, and potassium feldspar inclusions indicate monazite growth together with crystallization of the host granite. Thus, the age obtained defines the crystallization age of biotite granite and, accordingly, the time of diatexis coeval to the 2.76–2.70 Ga metamorphism of the Kola gneisses [45], which in turn could have been a source for S-type granites.

Local CHIME dating of primary monazite domains defines a similar age of 2734 ± 134 Ma (ThO_2*-PbO isochron). Secondary domains with curved boundaries and higher PbO and CaO contents most likely reflect late fluid-alteration processes. They yielded CHIME ages of 1796–1723 Ma that coincide with the widespread low-temperature hydrothermal alteration of rocks within the Kola region.

Monazite neoblastic domains yielded CHIME isochron ages of 2519–2550 Ma. Commonly, neoblastic monazite, formed by dynamic recrystallization, can be used to date tectonic and impact deformations because the recrystallization process forms new monazite free of inherited Pb [7,17,30]. The ages obtained are close to the 2.5 Ga age of the Jarva-Varaka Massif [26] and possibly reflect the influence of the Massif formation. In

monazite, the temperature necessary to activate nanoscale Pb mobility is 600 °C [46], and the Massif itself, as already mentioned, could hardly heat the host rocks up to 600 °C due to its small size. A hypothesis of the impact origin of the Jarva-Varaka structure would eliminate this contradiction.

According to BSE images, variation in ages (calculated according to Montel) and scatter of the data points at ThO_2*-PbO and UO_2*-PbO diagrams neoblastic domain also reflect lower-temperature fluid alteration, but due to the younger age, their structure is less disturbed by the radioactive decay of U and Th, and therefore they reacted to the fluid influence to a lesser extent than the host monazite grains.

6. Conclusions

Monazite-(Ce) from the sample of diatectite granite located among aluminous gneisses in the Jarva-Varaka structure contains multiple sets of twins along {100} and {001} with 180° disorientation relationships and plastically deformed domains with a maximum misorientation of 10°. Newly formed areas of recrystallization (neoblastic domains) that cut twins and plastically deformed subgrains were also documented.

Monazite grains yielded a U-Pb (ID-TIMS) age of 2706 ± 10 Ma, which reflects the crystallization of diatectite granite provided by the coeval 2.76–2.70 Ga metamorphism of the Kola gneisses. Local CHIME dating of primary monazite domains defines a similar age of 2734 ± 134 Ma (ThO_2*-PbO isochron). CHIME isochron ages of 1796–1723 Ma reflect late hydrothermal processes manifested in monazite. Monazite neoblastic domains yielded CHIME isochron ages of 2519–2550 Ma and are coeval to the 2.5 Ga Jarva-Varaka Massif.

Only two simple orientations of monazite twins, which can also occur in a tectonic setting, and the absence of shock-specific twins showed that the data obtained for monazite-(Ce) from diatectite granite are insufficient to confirm an impact origin of the Jarva-Varaka structure at this stage of the research and require further investigation.

Author Contributions: Conceptualization, T.K., L.N. and V.I.; methodology, V.S.; formal analysis, V.S., Y.S., L.L. and V.B.; investigation, T.K., V.S. and L.N.; writing—original draft preparation, T.K. and V.S. All authors have read and agreed to the published version of the manuscript.

Funding: The work was carried out in the framework of the State Contract of GI KSC RAS No. AAAA-A19-119100290148-4 (FMEZ-2022-0025).

Data Availability Statement: All the experiment and raw analysis data are available from authors on request. No data suitable for the generally used databases (such as crystal structures or high-resolution Raman spectra) was produced, the analytical data concerning the article's topic is fully provided in the text.

Acknowledgments: The authors are very grateful to the editor and reviewers for their considerate reading of the manuscript and numerous useful comments, which significantly helped to improve the manuscript. The authors would like to thank T. Ahmad for his help with English editing and the "Geomodel" resource center of SPbSU, grant No. 95439487.

Conflicts of Interest: The authors declare no conflict of interest.

References

1. Masaitis, V.L.; Danilin, A.N.; Mashchak, M.S.; Raikhlin, A.I.; Selivanovskaia, T.V.; Shadenkov, E.M. *Geology of Astroblemes*; Nedra: Leningrad, USSR, 1980; 231p. (In Russian)
2. Glikson, A.Y. *The Asteroid Impact Connection of Planetary Evolution*; Springer-Briefs: Dordrecht, The Netherlands, 2013; 150p.
3. Melosh, H.J. *Impact Cratering: A Geological Process*; Oxford University Press: New York, NY, USA, 1989; 245p.
4. Gibson, R.L.; Armstrong, R.A.; Reimold, W.U. The age and thermal evolution of the Vredefort impact structure: A single-grain U-Pb zircon study. *Geochim. Cosmoch. Acta* **1997**, *61*, 1531–1540. [CrossRef]
5. Davis, D.W. Sub-million year age resolution of Precambrian igneousevents by thermal extraction (TE-TIMS) Pb dating of zircon: Applicationto crystallization of the Sudbury impact melt sheet. *Geology* **2008**, *36*, 383–386. [CrossRef]
6. McDonald, F.A.; Bunring, J.A.; Cina, C.E. Yarrabubba—A large, deeply eroded impact structure in the Yilgarn Craton, Western Australia. *Earth Planet Sci. Lett.* **2003**, *213*, 235–247. [CrossRef]

7. Erickson, T.M.; Kirkland, C.L.; Timms, N.E.; Cavosie, A.J.; Davison, T.M. Precise radiometric age establishes Yarrabubba, Western Australia, as Earth's oldest recognized meteorite impact structure. *Nat. Commun.* **2020**, *11*, 300. [CrossRef]
8. Li, S.-S.; Keerthy, S.; Santosh, M.; Singh, S.P.; Deering, C.D.; Satyanarayanan, M.; Praveen, M.N.; Aneeshkumar, V.; Indu, G.K.; Anilkumar, Y.; et al. Anatomy of impactites and shocked zircon grains from Dhala reveals Paleoproterozoic meteorite impact in the Archean basement rocks of Central India. *Gondwana Res.* **2018**, *54*, 81–101. [CrossRef]
9. Mashchak, M.S.; Naumov, M.V. The Suavjärvi impact structure, NW Russia. *Meteorit. Planet Sci.* **2012**, *47*, 1644–1658. [CrossRef]
10. French, B.M. *Traces of Catastrophe: A Handbook of Shock-Metamorphic Effects in Terrestrial Meteorite Impact Structures*; Lunar and Planetary Institute: Houston, TX, USA, 1998; 130p.
11. Grieve, R.A.F. Extraterrestrial impacts on earth: The evidence and the consequences. In *Meteorites: Flux with Time and Impact Effects*; Grady, M.M., Hutchison, R., McCall, G.J.H., Rothery, D., Eds.; Geological Society, London, Special Publication: London, UK, 1998; Volume 140, pp. 105–131.
12. French, B.M.; Koeberl, C. The convincing identification of terrestrial meteorite impact structures: What works, what doesn't, and why. *Earth Sci. Rev.* **2010**, *98*, 123–170. [CrossRef]
13. Reimold, W.U.; Leroux, H.; Gibson, R.L. Shocked and thermally-metamorphosed zircon from the Vredefort impact structure, South Africa. *Eur. J. Mineral.* **2002**, *14*, 859–868. [CrossRef]
14. Gucsik, A.; Koeberl, C.; Brandstätter, F.; Reimold, W.U.; Libowitzky, E. Cathodoluminescence, electron microscopy, and Raman spectroscopy of experimentally shock-metamorphosed zircon. *Earth Planet Sci. Lett.* **2002**, *202*, 495–509. [CrossRef]
15. Gucsik, A.; Zhang, M.; Koeberl, C.; Salje, E.K.H.; Redfern, S.A.T.; Pruneda, J.M. Infrared and Raman spectra of ZrSiO4 experimentally shocked at high pressures. *Miner. Mag.* **2004**, *68*, 801–811. [CrossRef]
16. Wittmann, A.; Kenkmann, T.; Schmitt, R.T.; Stöffler, D. Shock-metamorphosed zircon in terrestrial impact craters. *Meteorit. Planet. Sci.* **2006**, *41*, 433–454. [CrossRef]
17. Erickson, T.M.; Cavosie, A.J.; Pearce, M.A.; Timms, N.E.; Reddy, S.M. Empirical constraints on shock features in monazite using shocked zircon inclusions. *Geology* **2016**, *44*, 635–638. [CrossRef]
18. Timms, N.E.; Erickson, T.M.; Pearce, M.A.; Cavosie, A.J.; Schmieder, M.; Tohver, E.; Reddy, S.M.; Zanetti, M.R.; Nemchin, A.A.; Wittmann, A. A pressure-temperature phase diagram for zircon at extreme conditions. *Earth Sci. Rev.* **2017**, *165*, 185–202. [CrossRef]
19. Cavosie, A.J.; Erickson, T.M.; Montalvo, P.; Prado, D.; Cintron, N.; Gibbon, R.J. *The Rietputs Formation in South Africa: A Pleistocene Fluvial Archive of Meteorite Impact Unique to the Kaapvaal Craton*; Microstructural geochronology; Lattice to Atom-Scale Records of Planetary Evolution. AGU Monograph; AGU-Wiley: Hoboken, NJ, USA, 2018; pp. 203–224.
20. Vishnevsky, S.A.; Pal'chik, N.A.; Moroz, T.N.; Leonova, I.V. Shock Metamorphism of Carbonaceous Matter in Impactites of the Janisjärvi Astrobleme, Karelia. *Dokl Earth Sci.* **2002**, *387A*, 1024–1027.
21. Huber, M.; Plado, J.; Ferrière, L. Oldest Impact Structures on Earth—The Case Study of the Suavjärvi Structure (Russia). *Large Meteor. Impacts Planet. Evol. V* **2013**, *1737*, 3073.
22. Nerovich, L.I.; Bayanova, T.B.; Kunakkuzin, E.L.; Bazai, A.V.; Nekipelov, D.A. New results of geological-petrographic and geochemical study of the stratified massif of Jarva-varaka, Monchegorsk ore area. *Proc. FSS GI KSC RAS* **2015**, *12*, 141–146. (In Russian)
23. Nerovich, L.I.; Kaulina, T.V.; Bayanova, T.B.; Ilchenko, V.L.; Kunakkuzin, E.L.; Bazai, A.V.; Mudruk, S.V.; Borisenko, E.S.; Sosnovskaya, M.F. Granophyre norites and diorites of the Jarva- Varaka massif (Monchegorsk ore area, Kola Region, Russia): Geology, petrography, geochemistry, geochronology and origin. *Geochem. Int.* **2023**, *61*, 572–592. [CrossRef]
24. Grieve, R.A.F. An impact model for the Sudbury structure. *Proc. Sudbury-Noril'sk Symp. Ont. Geol. Surv. Spec. Vol.* **1994**, *5*, 119–132.
25. Naldrett, A.J. *Magmatic Sulfide Deposits: Geology, Geochemistry, and Exploration*; Springer: Berlin, Germany, 2004; 727p.
26. Kaulina, T.V.; Nerovich, L.I.; Il'chenko, V.L.; Lialina, L.M.; Kunakkuzin, E.L.; Ganninbal, M.A.; Mudruk, S.V.; Elizarov, D.V.; Borisenko, E.S. Astroblems in the early Earth history: Precambrian impact structures of the Kola-Karelian region (East Baltic shield). In *Geological and Geo-Environmental Processes on Earth*; Springer: Singapore, 2021; pp. 25–37.
27. Schärer, U.; Deutsch, A. Isotope systematic and shock-wave metamorphism: II. U-Pb and Rb-Sr in naturally shocked rocks; the Haughton Impact Structure, Canada. *Geochim. Cosmoch. Acta* **1990**, *54*, 3435–3447. [CrossRef]
28. Silva, D.; Lana, C.; de Souza Filho, C.R. Petrographic and geochemical characterization of the granitic rocks of the Araguainha impact crater, Brazil. *Meteorit. Planet Sci.* **2016**, *51*, 443–467. [CrossRef]
29. Erickson, T.M.; Timms, N.E.; Kirkland, C.L.; Tohver, E.; Cavosie, A.J.; Pearce, M.A.; Reddy, S.M. Shocked monazite chronometry: Integrating microstructural and in situ isotopic age data for determining precise impact ages. *Contrib. Miner. Pet.* **2017**, *172*, 11. [CrossRef]
30. Fougerouse, D.; Cavosie, A.J.; Erickson, T.; Reddy, S.M.; Cox, M.A.; Saxey, D.W.; Rickard, W.D.A.; Wingate, M.T.D. A new method for dating impact events—Thermal dependency on nanoscale Pb mobility in monazite shock twins. *Geochim. Cosmochim. Acta* **2021**, *314*, 381–396. [CrossRef]
31. Moser, D.E. Dating the shock wave and thermal imprint of the giant Vredefort impact, South Africa. *Geology* **1997**, *25*, 7–10. [CrossRef]
32. Cavosie, A.J.; Quintero, R.R.; Radovan, H.A.; Moser, D.E. A record of ancient cataclysm in modern sand: Shock microstructures in detrital minerals from the Vaal River, Vredefort Dome, South Africa. *Bulletin* **2010**, *122*, 1968–1980. [CrossRef]

33. Kovaleva, E.; Dixon, R. Properties of Impact-Related Pseudotachylite and Associated Shocked Zircon and Monazite in the Upper Levels of a Large Impact Basin: A Case Study from the Vredefort Impact Structure. *Minerals* **2020**, *10*, 1053. [CrossRef]
34. Smolkin, V.F.; Fedotov, Z.A.; Neradovsky, Y.N.; Bayanova, T.B.; Borisova, V.V.; Glasnev, V.N.; Dedyukhin, A.N.; Orsoev, D.A.; Ohnenstetter, M.; Ohnenstetter, D.; et al. *Layered Intrusions of the Monchegorsk Ore Region: Petrology, Mineralization, Isotopy, Deep Structure*; KSC RAS: Apatity, Russia, 2004; 177p. (In Russian)
35. Sosnovskaya, M.A.; Nerovich, L.I. Petrographic and petrochemical characterization of gneisses and granitoids framing the Jarva-varaka massif. *Proc. FSS GI KSC RAS* **2020**, *17*, 515–519. (In Russian)
36. Krogh, T.E. A low-contamination method for hydrothermal decomposition of zircons and extraction of U and Pb for isotopic age determinations. *Geochim. Cosmochim. Acta* **1973**, *37*, 485–494. [CrossRef]
37. Kaulina, T.V.; Kalinin, A.A.; Il'chenko, V.L.; Gannibal, M.A.; Avedisyan, A.A.; Elizarov, D.V.; Nerovich, L.I.; Nitkina, E.A. Age and Formation Conditions of U Mineralization in the Litsa Area and the Salla-Kuolajarvi Zone (Kola Region, Russia). *Minerals* **2018**, *8*, 563. [CrossRef]
38. Suzuki, K.; Adachi, M. Precambrian provenance and Silurian metamorphism of the Tsubonosawa paragneiss in the South Kitakami terrane, Northeast Japan, revealed by the chemical Th-U-total Pb isochron ages of monazite, zircon and xenotime. *Geochem. J.* **1991**, *25*, 357–376. [CrossRef]
39. Montel, J.-M.; Foret, S.; Veschambre, M.; Nicollet, C.; Provost, A. Electron microprobe dating of monazite. *Chem. Geol.* **1996**, *131*, 37–53. [CrossRef]
40. Votyakov, S.L.; Shchapova, Y.V.; Hiller, V.V. *Crystal Chemistry and Physics of Radiation-Thermal Effects in a Number of U-Th-Containing Minerals as a Basis for Their Chemical Microprobe Dating*; IGG UB RAS: Ekaterinburg, Russia, 2011; 336p. (In Russian)
41. Ludwig, K.R. *User's Manual for Isoplot Version 3.75–4.15: A Geochronological Toolkit for Microsoft Excel*; Berkeley Geochronology Center: Berkeley, CA, USA, 2012; p. 5, Special Publication.
42. Erickson, T.M.; Pearce, M.A.; Taylor, R.J.M.; Timms, N.E.; Clark, C.; Reddy, S.M.; Buick, I.S. Deformed monazite yields high-temperature tectonic ages. *Geology* **2015**, *43*, 383–386. [CrossRef]
43. Hay, R.; Marshall, D. Deformation twinning in monazite. *Acta Mater.* **2003**, *51*, 5235–5254. [CrossRef]
44. Schulz, B.; Lange, J.-M.; Krause, J.; Czygan, D. Monazite in lithoclasts of suevite impact breccia in the Nördlinger Ries (Bavaria, Germany) and its Th-U-Pb dating by electron probe microanalysis. *Z. Dtsch. Ges. Geowiss.* **2022**. [CrossRef]
45. Levchenkov, O.A.; Levsky, L.K.; Nordgulen, Ø.; Dobrzhinetskaya, L.F.; Vetrin, V.R.; Cobbing, J.; Nilsson, L.P.; Sturt, B.A. U-Pb zircon ages from Sörvaranger, Norway and the western part of the Kola Peninsula, Russia. *Nor. Geol. Unders. Spec. Publ.* **1995**, *7*, 29–47.
46. Gardés, E.; Jaoul, O.; Montel, J.-M.; Seydoux-Guillaume, A.-M.; Wirth, R. Pb diffusion in monazite: An experimental study of $Pb^{2+}Th^{4+} = 2Nd^{3+}$ interdiffusion. *Geochim. Cosmochim. Acta* **2006**, *70*, 2325–2336. [CrossRef]